Controlling the morphology of yttrium oxide through different precursors synthesized by hydrothermal method

Nan Li and Kazumichi Yanagisawa*

Research Laboratory of Hydrothermal Chemistry, Faculty of Science, Kochi University, 2-5-1 Akbono-cho, Kochi 780-8520, Japan

* Corresponding author. Phone: 088-844-8352. Fax: 088-844-8362. E-mail: yanagi@cc.kochi-u.ac.jp.

Abstract

Y_2O_3 sheets, rods, needles and tubes were synthesized from three precursors through hydrothermal reactions followed by calcination. The phase distribution and decomposition behaviors of the three precursors, $Y_2(OH)_{5.14}(NO3)_{0.86}{\cdot}H_2O$, $Y_4O(OH)_9(NO_3)$ and hexagonal $Y(OH)_3$, were investigated. The reaction temperature and initial pH value during the hydrothermal reaction showed great influence on the shape and particle size of the products. The precursors were converted to Y_2O_3 particles with the retained original morphology of the precursors.

Keywords: Yttrium nitrate hydroxide hydrate; Yttrium oxide nitrate hydroxide; Yttrium hydroxide; Yttrium oxide; Hydrothermal synthesis.

1. Introduction

Yttrium oxide is one of the most important rare-earth compounds and has been used in a broad range of fields such as optics, advanced ceramics, optoelectronics, catalytic reactions, as well as high-efficient additives for functional composite materials. Industrially, yttrium oxide is produced by solid state decomposition reaction at high temperatures. Gas-phase condensation [1], precipitation [2], sol-gel processing [3], combustion [4], pyrolysis [5], and recently, hydrothermal synthesis [6-17] are other physical and chemical techniques for preparation of yttrium oxide include

Hydrothermal synthesis is widely accepted as a simple and mild method to prepare high crystalline materials with controlled particle size. Recently, the hydrothermal synthesis of yttrium oxide attracted increasing attention owing to the prospects of producing high-quality, well-dispersed crystals as well as the convenience in preparing homogeneous doped materials. According to the phase diagram of Y_2O_3-H_2O system [18], Y_2O_3 is not stable under hydrothermal conditions at temperature lower than 550 °C, so that the products of hydrothermal reaction are normally precursors of yttrium oxide rather than oxide itself. The precursors decompose into the oxide through heat treatments. The most familiar precursor is hexagonal yttrium hydroxide [6-12]. In addition, yttrium oxide nitrate hydroxide, $Y_4O(OH)_9(NO_3)$, is also reported [13-14]. Similar procedures were employed in most of the published reports on synthesis of yttrium oxide, which involve hydrothermal treatment of a colloidal precipitate followed by subsequent calcination. However, most of these researches focused on the final product, i.e. yttrium oxide, and little information on precursors was given, although precursors play important roles on final products. Moreover, despite the similarities in synthesis procedure, dissimilar results were reported. For

example, the reported sizes of yttrium oxide range from several nanometers to tens of micrometers, and various shapes like spherical particle [6, 15], rod or wire [6-7, 16-17], tube [8-11, 15, 17], belt [7, 13], trilobal prism [14], and plate [6, 15-16] were described. All of these bewildering results trigger a critical demand for a comprehensive investigation on hydrothermal synthesis of yttrium-based compounds. Herein, we selected the phase distribution and morphology of precursors as the point of our research and examined the influences of correlative factors on them.

2. Experimental section

All chemicals were purchased from Wako pure chemical industries, Ltd. (Japan) and used without purification. In a typical synthesis process, 0.45 g of Y_2O_3 was dissolved in 6 ml of 3.0 M nitric acid solution under heating. Then ammonia solution (or NaOH solution) was added to adjust the solution to a designated pH value under vigorous agitation. The volume of the resulting solution was adjusted to around 15 ml. (In order to adjust pH value in a wide range from 6.0 to 14.0 and maintain the solution volume an approximate constant at the same time, basic solutions with different concentrations were used. When ammonia solution was used as a base, solutions with pH value higher than 12.0 were prepared by centrifuging the solution with pH ~12.0 followed by redispersing the precipitate in concentrated ammonia solutions.) The as-obtained colloidal solution was transferred into a 25 ml Teflon-lined autoclave, followed by hydrothermal treatment at temperature of 80-220 ºC for 24 h. After cooling, the received white precipitate was collected by centrifuge, then washed with distilled and dried at room temperature. Finally, it was calcined at 600 ºC for 4 h in air.

Powder X-ray diffractions (XRD) were measured on a Rigaku RTP-300RC diffractometer using Cu Kα radiation (λ = 1.54056 Å) operating at voltage and current of 40 kV and 100 mA,

respectively. The patterns were collected in the range of 5-70 º in 2 θ/θ scanning mode with a 0.02 º step and scanning speed of 4 º/min. Micrographs of scanning electron microscopy (SEM) and transmission electron microscopy (TEM) were obtained using Hitachi S-530 electron microscope operating at 25 kV and Hitachi H-800 electron microscope operating at 200 kV, respectively. The average particle size and size distribution were determined from about one hundred particles in microphotographs. A SSC5200 thermal analysis system with Seiko TG/DTA 320 module was used for the thermogravimetric analysis. Samples were heated in air with a ramp rate of 5 ºC/min. The content of NO_3^- of the samples heated at different temperatures was measured using a Dionex DX-120 ion-chromatograph analyzer. The samples were dissolved in 5 ml of 1 mol/L H_2SO_4 and then diluted to 50 ml.

3. Results and discussion

3.1 Phase distribution and decomposition behaviors of Y_2O_3 precursors

When NH_4OH was used as a base, three main compounds were obtained in the range of our experimental conditions from 80 ºC to 220 ºC and from pH 6.0 to pH 13.5. The phase distribution diagram and typical XRD patterns of these compounds are shown in Figure 1 and Figure 2, respectively. The phase distribution was indicated by the temperature and initial pH value of hydrothermal reaction. It can be seen from the diagram that when reaction temperature was below 90 ºC, two compounds were obtained. The first one was received under neutral to weak basic condition, and its XRD peaks were well matched with the reported data of a kind of hydrated yttrium nitrate hydroxides, $Y_2(OH)_{5.14}(NO_3)_{0.86}\cdot H_2O$ (JCPDS 32-1435). At higher pH value, hexagonal yttrium hydroxide, $Y(OH)_3$, was obtained. The pH boundary line between these two phases was around 11.25. When temperature increased beyond 90 ºC, another compound was formed near the pH boundary. Its XRD peaks can be indexed to a monoclinic lattice of yttrium

oxide nitrate hydroxide, $Y_4O(OH)_9(NO_3)$ (JCPDS 79-1352). As reaction temperature increased, the formation region of $Y_4O(OH)_9(NO_3)$ extended to lower pH value. Accordingly, the formation region of $Y_2(OH)_{5.14}(NO_3)_{0.86}\cdot H_2O$ phase narrowed down and $Y_2(OH)_{5.14}(NO_3)_{0.86}\cdot H_2O$ was not obtained when reaction temperature exceeded 210 ºC. In contrast to this result, the pH value at which hexagonal yttrium hydroxide appeared did not change much with increasing temperature. Except for the three compounds mentioned above, a small amount of monoclinic $Y(OH)_3$ with flake shape coexisted with $Y_4O(OH)_9(NO_3)$ or hexagonal $Y(OH)_3$ at relatively high temperature and high pH value.

Compared with that of $Y_2(OH)_{5.14}(NO_3)_{0.86}\cdot H_2O$, the structure of $Y_4O(OH)_9(NO_3)$ has high OH/NO_3 ratio. As the concentration of NO_3^- in the solution is maintained to be a constant, products with higher content of hydroxyl are preferable under high OH^- concentration, which accounts for the transformation from $Y_2(OH)_{5.14}(NO_3)_{0.86}\cdot H_2O$ to $Y_4O(OH)_9(NO_3)$ as pH value increased. The temperature dependent feature of this transformation is due to the high stability of $Y_4O(OH)_9(NO_3)$ without hydrated water at high temperatures. The higher hydroxyl concentration at elevated temperature resulted from the enhanced dissociation of water could partly account for the high-temperature stability of $Y_4O(OH)_9(NO_3)$. Similarly, when the pH value of solution is further increased, yttrium hydroxide, which contains more hydroxyl in the structure, is obtained.

In order to investigate the role of base in the hydrothermal synthesis of yttrium compounds, sodium hydroxide was employed to replace NH_4OH for comparison. Figure 3 shows the distribution diagram of NaOH system. The main products as well as the tendency of transformation between phases are identical for both bases. But the phase formation regions in NaOH system differ from those in ammonia solution. First of all, the lowest synthesis temperature of $Y_4O(OH)_9(NO_3)$ increased from 90 °C to 120 °C. Moreover, $Y_4O(OH)_9(NO_3)$ or

$Y_2(OH)_{5.14}(NO_3)_{0.86}·H_2O$ did not transform into hexagonal $Y(OH)_3$ until initial pH value increased to 13.0. The pH boundary was much higher than that in NH_4OH system, where hexagonal $Y(OH)_3$ appeared at pH of ~11.25. This difference arises from the different features of strong base and weak base. When the pH value of ammonia solution and NaOH solution reaches equal, excess ammonium hydroxide is involved in the solution, existing as an undissociated state. When the progress of reaction and the depletion of the hydroxyl ion proceed, the ammonium hydroxide is further dissociated to maintain the pH value of solutions an approximate constant. This is confirmed by the final pH value of solutions. When ammonia solution was used as a base, the pH value did not show significant change after hydrothermal reaction. In the case of NaOH system, when initial pH was lower than 13.0, the dropping of pH value to 6-7 was observed. At pH higher than 13.0, the pH value did not change so much, which suggests that the amount of NaOH is in excess for the formation of hydroxide.

The thermal behaviors of the three compounds in air were studied by TG-DTA, as shown in Figure 4. The decomposition profile of $Y_2(OH)_{5.14}(NO_3)_{0.86}·H_2O$ is fairly complex with overlapping steps. Ion chromatography analysis indicated that the NO_3^- content in intermediate products at different calcination steps kept increasing when calcination temperature was lower than 450 °C, while it decreased dramatically during 450 °C to 530 °C. Combined with the theoretical weight loss, it can be concluded that the weight loss of 19.11% below 450 °C corresponds to the evaporation of water (expected weight loss: 19.1%), while the weight loss at higher temperature is associated with the release of N-O species. The overall weight loss of 32.95% is consistent well with the theoretical value of 32.9%. For $Y_4O(OH)_9(NO_3)$, it underwent two decomposition steps. Similar as that of $Y_2(OH)_{5.14}(NO_3)_{0.86}·H_2O$, the NO_3^- content of intermediate products did not decrease until temperature increased to 460 °C, which indicates that N-O species were released in the second step. The weight loss of the first step at

temperatures from 330 °C to 450 °C is 10.14%, which is lower than the theoretical value of the total release of water (13.8%). This suggests that some hydroxyl is stilled remained in the structure. In the second step, the sample was transformed into oxide at ~ 490 °C with the release of N-O species and water. For hexagonal $Y(OH)_3$, a stepwise decomposition also occurred with near-plateaus on the TG curves. The weight loss below 350 °C is 12.35%, which corresponds to the transformation of hydroxide to oxyhydroxide, YOOH (expected weight loss: 12.9%). YOOH further decomposed into Y_2O_3 by releasing water. This result is consistent with that given by Sato et al [19]. In the DTA curves, the last endothermic peaks were observed at 525, 490, 415 °C for $Y_2(OH)_{5.14}(NO_3)_{0.86}\cdot H_2O$, $Y_4O(OH)_9(NO_3)$, and hexagonal $Y(OH)_3$, respectively. These results indicated that the formation temperature of Y_2O_3 decreases with increasing content of hydroxyl group in the molecules. A typical XRD pattern of the resulting yttrium oxide is shown in Figure 2d. All peaks belong to cubic phase of Y_2O_3 (JCPDS 41-1105). No significant difference was observed in the XRD patterns of the oxides derived from different precursors.

3.2 Y_2O_3 sheets

Figure 5 shows the SEM and TEM images of Y_2O_3 derived from $Y_2(OH)_{5.14}(NO_3)_{0.86}\cdot H_2O$ precursor prepared in NH_4OH system. It can be seen that the oxide obtained from the precursor synthesized at 100 ºC and pH 7.5 is composed of sheets with irregular edges.[1] Its lateral size ranges from 70 to 370 nm and thickness is around 37 nm (Figure 5a). The oxide sheets maintained the morphology of precursor except for slight size shrinkage due to the higher density of oxide than that of the precursor. When initial pH value during hydrothermal reaction was increased, the sheet size decreased dramatically. Figure 5b shows the Y_2O_3 nanoflakes prepared at pH 10.5 at the same temperature. They are sintered a little and seem to be porous compared with the precursor (inset). Besides pH value, reaction temperature is also observed to have a

strong effect on the morphological features of products. As reaction temperature increased, the edges of these sheets sharpened and lateral size as well as thickness increased. Figure 5c shows the product synthesized at 160 ºC with pH 7.5, which is composed of hexagonal/rhombic microsheets with lateral size of 1-4 μm and thickness of about 150 nm. When pH value was carefully controlled between 6.0-6.5, regular hexagonal sheets with lateral size of 15-30 μm and thickness of 0.6-1.1 μm could be prepared at temperature as high as 200 ºC. In NaOH system, the morphology of product changed in the same way.

The effects of pH value and reaction temperature on product size are related to the nucleation and growth process of the particles. In NH_4OH system, with the addition of ammonia solution, the pH value of yttrium nitrate solution increased and a white colloidal precipitation formed as pH value exceeded 6.0. Previous study [20] shows that the precipitate is hydrated yttrium nitrate hydroxide of the general formula $Y(OH)_{3-x}(NO_3)_x \cdot yH_2O$. The value of x decreases with the increasing pH, and at higher pH value amorphous yttrium hydroxide, $Y(OH)_3 \cdot yH_2O$, is formed. In the subsequent hydrothermal reactions, these amorphous yttrium nitrate hydroxides or yttrium hydroxide dissolve in the solution at elevated temperatures and then crystallize into yttrium compounds with definite compositions. The shape and size of products are closely related to the nucleation process, which is strongly affected by the solubility of the product in the precipitating solution. An increase in OH^- concentration decreases the solubility of product remarkably, which leads to a rapid supersaturation of the solution and a large amount of nuclei are formed at the same time. Thus, the growth for each seed is suppressed due to the rapid decrease of supersaturation, resulting in the formation of small-sized products. On the other hand, the solubility of product is increased significantly by increasing reaction temperature. As a result, supersaturation to lead nucleation decreases and the growth of existing particles is favored over nucleation of new precipitate particles, which results in formation of big particles.

3.3 Y_2O_3 rods

Y_2O_3 derived from $Y_4O(OH)_9(NO_3)$ is in rod shape with hexagonal cross-section. It was found that rod size was sensitive to the initial pH value of starting solutions. High pH value gave small particles. Taking the products synthesized at 200 ºC in NH_4OH system for example, the average length of the product synthesized at pH 6.5 was about 131 μm, which gradually reduced to 113 μm, 32 μm, 1.1 μm, 0.8 μm and 0.4 μm as pH value increased to 7.5, 8.5, 9.5, 10.5 and 11.0, respectively. The aspect ratio is in the range of 5.3~8.0. The particle size ranges from sub-millimeter scale to sub-micrometer scale, covering more than two orders of magnitude. Figure 6a and 6b show the typical SEM images of Y_2O_3 micorods synthesized at pH 8.5 and pH 10.5. The influence of pH value on rod size is the same as that for Y_2O_3 sheets derived from $Y_2(OH)_{5.14}(NO_3)_{0.86}\cdot H_2O$ precursor. High pH value leads to the formation of large amount of nuclei and small particles are favored due to the suppressed growth of each nuclear. It was found that decrease in initial concentration also resulted in small-sized products. Figure 6c shows the nanowires synthesized from solution with initial yttrium concentration half of that for Y_2O_3 micorods. The average diameter of these nanowires is around 50 nm and the length is up to several micrometers. We also investigated the effect of hydrothermal temperature on products. When pH value was fixed to 10.5 and the reaction temperature was in the range of 140 °C-220 °C, products did not show much difference in morphology except for the size distribution narrowed down with increasing temperature. This result shows that pH value is the predominant factor in strong basic media and the morphologies are less dependent on reaction temperature as compared with pH value.

3.4 Y_2O_3 needles and tubes

Needle-like Y_2O_3 could be prepared from hexagonal $Y(OH)_3$ precursor. Figure 7 shows the Y_2O_3 needles synthesized at pH value of 12.0 with width of 40-100 nm and length up to 1.4 μm. This morphology is familiar for hexagonal $Y(OH)_3$. Many researches [8-11, 17] have previously reported the synthesis of $Y(OH)_3$ and corresponding Y_2O_3 nanotubes under strong basic conditions using NaOH or KOH as base. We supposed that similar structures could be prepared in ammonia solution as long as high pH value was achieved. In order to obtain high pH value in an ammonia solution, the precipitate collected by centrifuge from the solution with pH 12.0 was redispersed in 25% ammonia to achieve a solution with pH value as high as 13.5. As expected, tubular products were obtained after hydrothermal reaction. Figure 8a shows an individual Y_2O_3 tube synthesized at 160°C, which shows outer diameter of ~98 nm and wall thickness of ~18 nm. The tips of the tube are open and the middle part is blocked. This structural feature could be seen more clearly from the images of its precursor, hexagonal $Y(OH)_3$, as shown in Figure 8b-d. It is interesting to note that reaction temperature also play an important role in the formation of $Y(OH)_3$ nanotubes. At the same pH value of 13.5, $Y(OH)_3$ crystals synthesized at 200 °C were in needle shape. While at lower temperature of 100 °C, tubes with less regular tips were obtained, as shown in Figure 8e. These results indicate that nanoneedles are more stable than nanotubes at high temperatures. This phenomenon was also observed by Wang for yttrium hydroxide and other rare-earth hydroxides [21].

Although the growth process of the $Y(OH)_3$ nanotubes is still unclear, some useful information can be acquired from the synthesis method and morphological characteristics of these nanotubes. It is apparent that the growth is not catalyst-assisted or surfactant-directed process, because the synthetic route adopted in this study involves neither catalyst nor surfactant. Open ends is a unique feature for nanotubes grown by rolling of lamellar structures, like C [22], BN [23], WS_2 [24], and so on. The nanotubes formed through that process normally possess hollow interior

throughout the tube axis. The blocked interior of our products indicates this mechanism is not the case for $Y(OH)_3$ nanotubes. Two possible mechanisms can be used to explain the formation of nanotubes with open ends and blocked interior. (1) Firstly, nanostructured particles (like particle, plate, or rod) are formed as seeds, and then subsequent preferential growth along the circumferential edges of the seeds gives a tubular structure. A similar mechanism proposed by Tang [8] has been used to account for the formation of $Y(OH)_3$ nanotubes in the presence of polyethylene glycol. (2) 1D nanostructured particles (like rod, needle) are formed at first, and then the central part of these particles is selectively dissolved to form hollow interior. This phenomenon was observed by Tong et al. in the growth of ZnO nanotubes [25]. In their study, the polar surfaces having the higher energy of the ZnO nanotowers were dissolved in priority to decrease the system energy in the aging process, and resulted in formation of tubular structure. Considering the lower stability of tubular $Y(OH)_3$ in comparison with that of needlelike structure, the former mechanism is more reasonable.

4. Conclusion

Y_2O_3 particles with controlled morphology and size were prepared from three yttrium compounds, $Y_2(OH)_{5.14}(NO_3)_{0.86}\cdot H_2O$, $Y_4O(OH)_9(NO_3)$ and hexagonal $Y(OH)_3$ through hydrothermal reactions followed by heat treatments at 600 ºC. The chemical composition of precursors as well as the morphologies of products is closely related to the hydrothermal reaction conditions. By simply adjusting the hydrothermal temperature and initial pH value of the starting solution, products with a diversity of well-defined morphologies like sheet, rod, needle and tube were successfully fabricated from different precursors. At the same time, the particle size of products could be controlled in a wide range.

References and Notes

[1] D. K. Williams, H. Yuan, B. M. Tissue, J. Lumin. 83 (1999) 297-300.

[2] C. J. J. Tool, E. H. P Cordfunke, Solid State Ionics 32/33 (1989) 691-697.

[3] A. Dupont, C. Parent, B. Le Garrec, J. M. Heintz, J. Solid State Chem. 171 (2003) 152-160.

[4] H. Song, B. Chen, H Peng, J. Zhang, Appl. Phys. Lett. 81 (2002) 1776-1778.

[5] A. J. Rulison, R. C. Flagan, J. Am. Ceram. Soc. 77 (1994) 3244-3250.

[6] Q. Li, C. Feng, Q. Jiao, L. Guo, C. Liu, H. B. Xu, Phys. Stat. Sol. A 201 (2004) 3055-3059.

[7] X. Wu, Y. Tao, F. Gao, L. Dong, Z. Hu, J. Cryst. Growth 277 (2005) 643-649.

[8] Q. Tang, Z. Liu, S. Li, S. Zhang, X. Liu, Y. Qian, J. Cryst. Growth 259 (2003) 208-214.

[9] X. Wang, X. Sun, D. Yu, B. Zou, Y. Li, Adv. Mater. 15 (2003) 1442-1445.

[10] Y. P. Fang, A. W. Xu, L. P. You, R. Q. Song, J. C. Yu, H. X. Zhang, Q. Li, H. Q. Liu, Adv. Funct. Mater. 13 (2003) 955-960.

[11] W. Li, X. Wang, Y. Li, Chem. Commun. (2004) 164-165.

[12] C. Hu, Z. Gao, J. Mater. Sci. 41 (2006) 6126-6129.

[13] Y. He, Y. Tian, Y. Zhu, Chem. Lett. 32 (2003) 862-863.

[14] J. Zhang, Z. Liu, J. Lin, J. Fang, Cryst. Growth Des. 5 (2005) 1527-1530.

[15] G. De, W. Qin, J. Zhang, J. Zhang, Y. Wang, C. Cao, Y. Cui, Solid State Commun. 137 (2006) 483-487.

[16] J. Wan, Z. Wang, X. Chen, L. Mu, Y. Qian, J. Cryst. Growth 284 (2005) 538-543.

[17] X. Bai, H. Song, L. Yu, L. Yang, Z. Liu, G. Pan, S. Lu, X. Ren, Y. Lei, L. Fan, J. Phys. Chem. B 109 (2005) 15236-15242.

[18] M. W. Shafer, R. Roy, J. Am. Ceram. Soc. 42 (1959) 563-570.

[19] T. Sato, S. Imaeda, K. Sato, Thermochim. Acta 133 (1988) 79-85.

[20] I. Schildermans, J. Mullens, J. Yperman, D. Franco, L. C. Van Poucke, Thermochim. Acta 231 (1994) 185-192.

[21] X. Wang, Y. Li, Chem. Eur. J. 9 (2003) 5627-5635.

[22] S. Amelinckx, D. Bernaerts, X. B. Zhang, G. Van Tendeloo, J. Van Landuyt, Science 267 (1995) 1334-1338.

[23] N. G. Chopra, R. J. Luyken, K. Cherrey, V. H. Crespi, M. L. Cohen, S. G. Louie, A. Zettl, Science 269 (1995) 966-967.

[24] R. Tenne, L. Margulis, M. Genut, G. Hodes, Nature 360 (1992) 444-446.

[25] Y. Tong, Y. Liu, C. Shao, Y. Liu, C. Xu, J. Zhang, Y. Lu, D. Shen, X. Fan, J. Phys. Chem. B 110 (2006) 14714-14718.

Footnotes

1. For the sake of simplicity, the parameters during hydrothermal reaction were used to describe the synthesis condition of yttrium oxide, although hydrothermal reaction will not result in yttrium oxide directly.

Figure captions

Fig. 1. Phase distribution in temperature-pH diagram for NH_4OH system. Symbol ●, ×, and ◊ represents $Y_2(OH)_{5.14}(NO_3)_{0.86}·H_2O$, $Y_4O(OH)_9(NO_3)$ and hexagonal $Y(OH)_3$, respectively.

Fig. 2. Typical XRD patterns of (a) $Y_2(OH)_{5.14}(NO_3)_{0.86}·H_2O$, (b) $Y_4O(OH)_9(NO_3)$, (c) hexagonal $Y(OH)_3$ and (d) Y_2O_3. Hydrothermal condition: (a) 160 °C, pH 7.5, NH_4OH system, (b) 200 °C, pH 9.5, NH_4OH system, (c) 200 °C, pH 12.0, NH_4OH system. Sample (d) was derived from sample (b) by calcining at 600 °C for 4h.

Fig. 3. Phase distribution in temperature-pH diagram for NaOH system. Symbol ●, ×, and ◊ represents $Y_2(OH)_{5.14}(NO_3)_{0.86}·H_2O$, $Y_4O(OH)_9(NO_3)$ and hexagonal $Y(OH)_3$, respectively.

Fig. 4. TG-DTA curves of (a) $Y_2(OH)_{5.14}(NO_3)_{0.86}·H_2O$, (b) $Y_4O(OH)_9(NO_3)$ and (c) hexagonal $Y(OH)_3$. Hydrothermal condition: (a) 160 °C, pH 7.5, NH_4OH system, (b) 200 °C, pH 9.5, NH_4OH system and (c) 200 °C, pH 12.0, NH_4OH system.

Fig. 5. SEM/TEM images of Y_2O_3 sheets obtained from $Y_2(OH)_{5.14}(NO_3)_{0.86}·H_2O$ precursors synthesized in NH_4OH system under various hydrothermal conditions: (a) 100 °C, pH 7.5, (b) 100 °C, pH 10.5, (c) 160 °C, pH 7.5, and (d) 200 °C, pH 6.3. Inset: TEM image of corresponding $Y_2(OH)_{5.14}(NO_3)_{0.86}·H_2O$ precursor.

Fig. 6. SEM/TEM images of Y_2O_3 microrods and nanowires obtained from $Y_4O(OH)_9(NO_3)$ precursors synthesized under various hydrothermal conditions: (a) 200 °C, pH 8.5, NH_4OH system, (b) 200 °C, pH 10.5, NH_4OH system and (c) 200 °C, pH 12.5, NaOH system, with half initial yttrium concentration as described in the experimental section . Inset: corresponding $Y_4O(OH)_9(NO_3)$ precursor.

Fig. 7. TEM image of Y_2O_3 needles obtained from $Y(OH)_3$ precursors synthesized at 200 °C and pH 12.0 in NH_4OH system. Inset: TEM image of corresponding hexagonal $Y(OH)_3$ precursor.

Fig. 8. TEM images of Y_2O_3 nanotube (a) obtained from $Y(OH)_3$ precursors and hexagonal $Y(OH)_3$ nanotubes (b)-(e). Hydrothermal condition: (a)-(d) 160 °C, pH 13.5 in NH_4OH system; (e) 100 °C under the same condition.

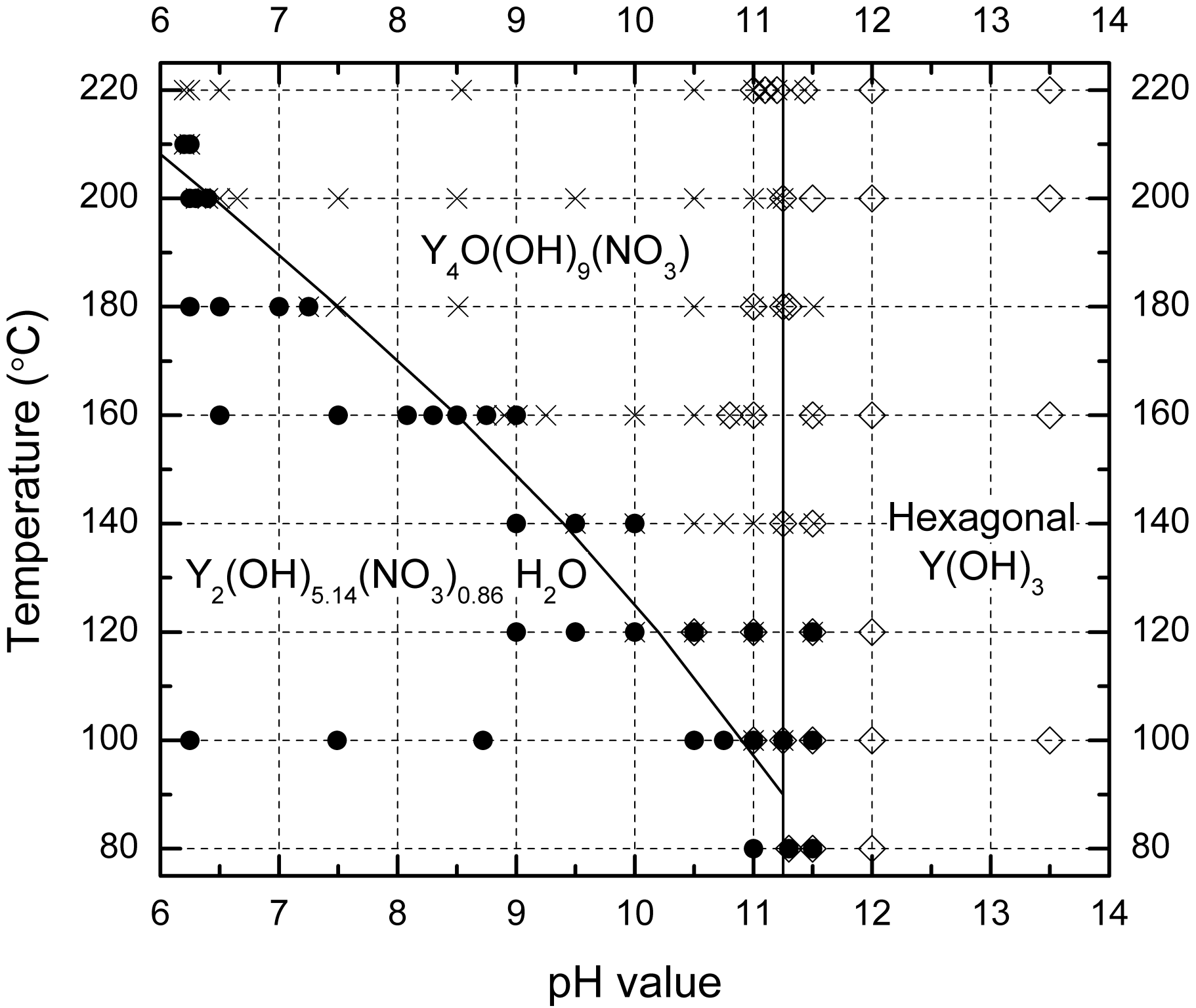
6
7
8
9
10
11
12
13
14
220
200
180
160
140
120
100
80
Temperature (°C)
pH value
$Y_4O(OH)_9(NO_3)$
$Y_2(OH)_{5.14}(NO_3)_{0.86}\ H_2O$
Hexagonal
$Y(OH)_3$

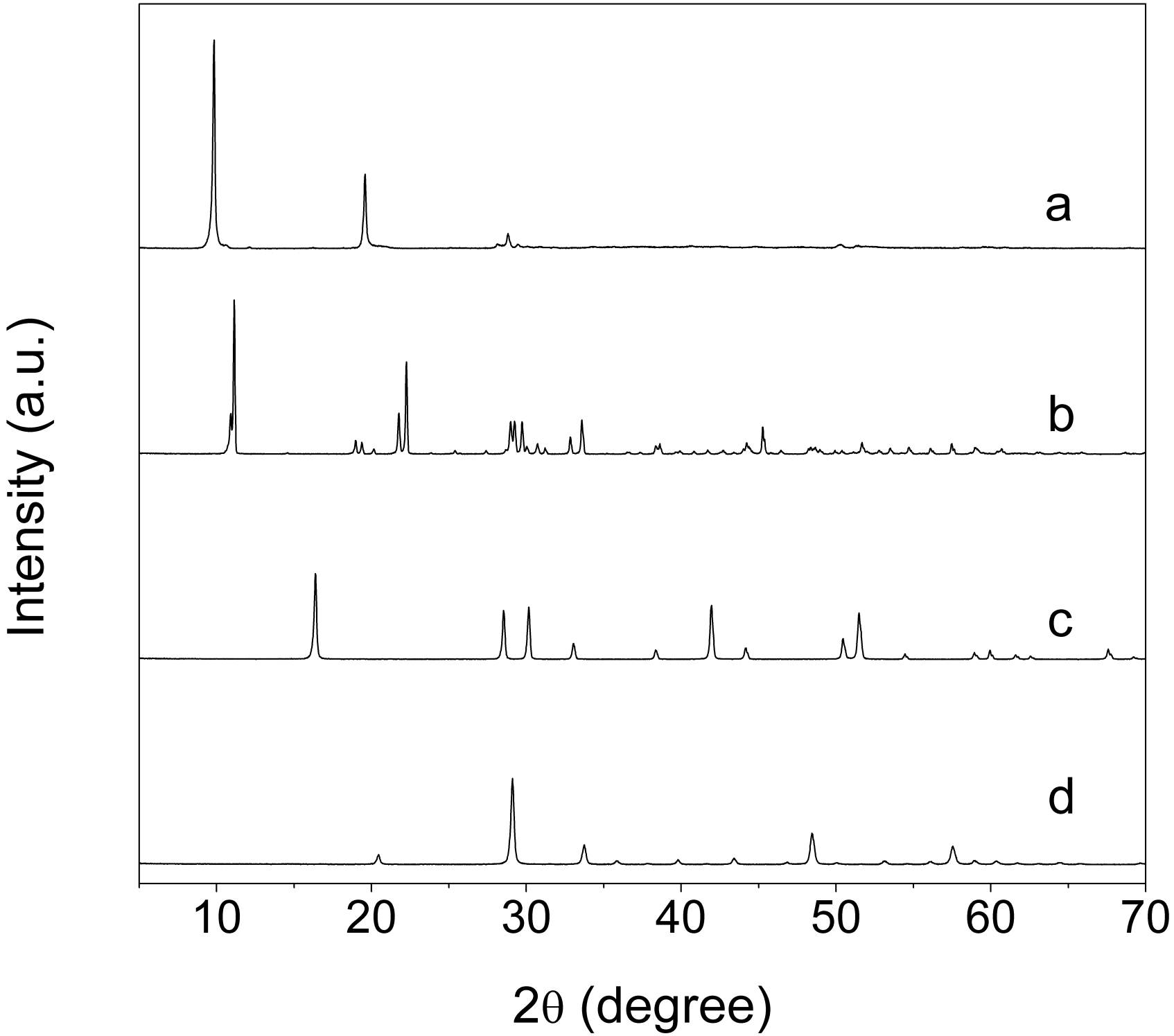
Intensity (a.u.)
a
b
c
d
10
20
30
40
50
60
70
2θ (degree)

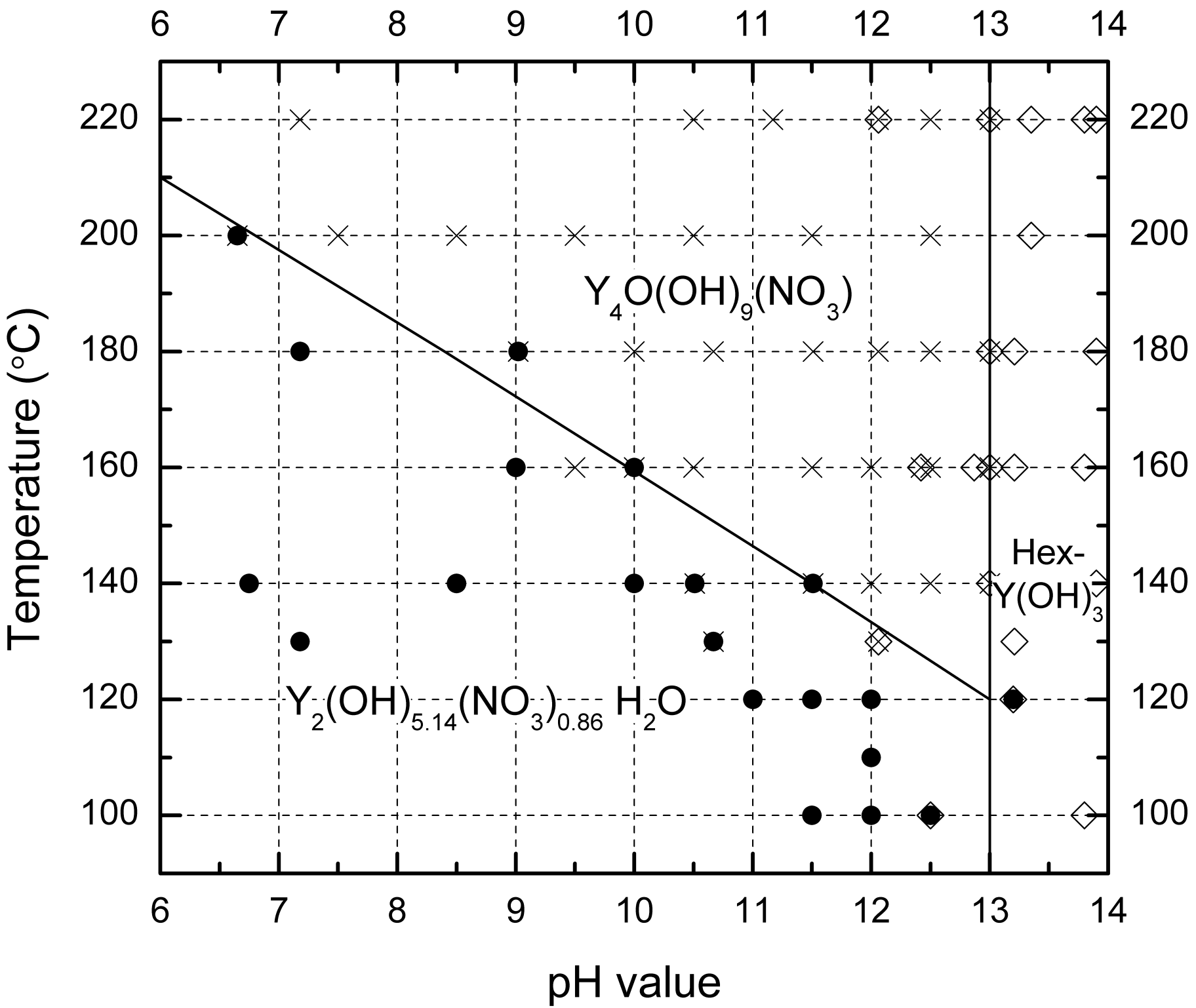
6
7
8
9
10
11
12
13
14
220
200
180
160
140
120
100
Temperature (°C)
pH value
$Y_4O(OH)_9(NO_3)$
Hex-
$Y(OH)_3$
$Y_2(OH)_{5.14}(NO_3)_{0.86}\ H_2O$

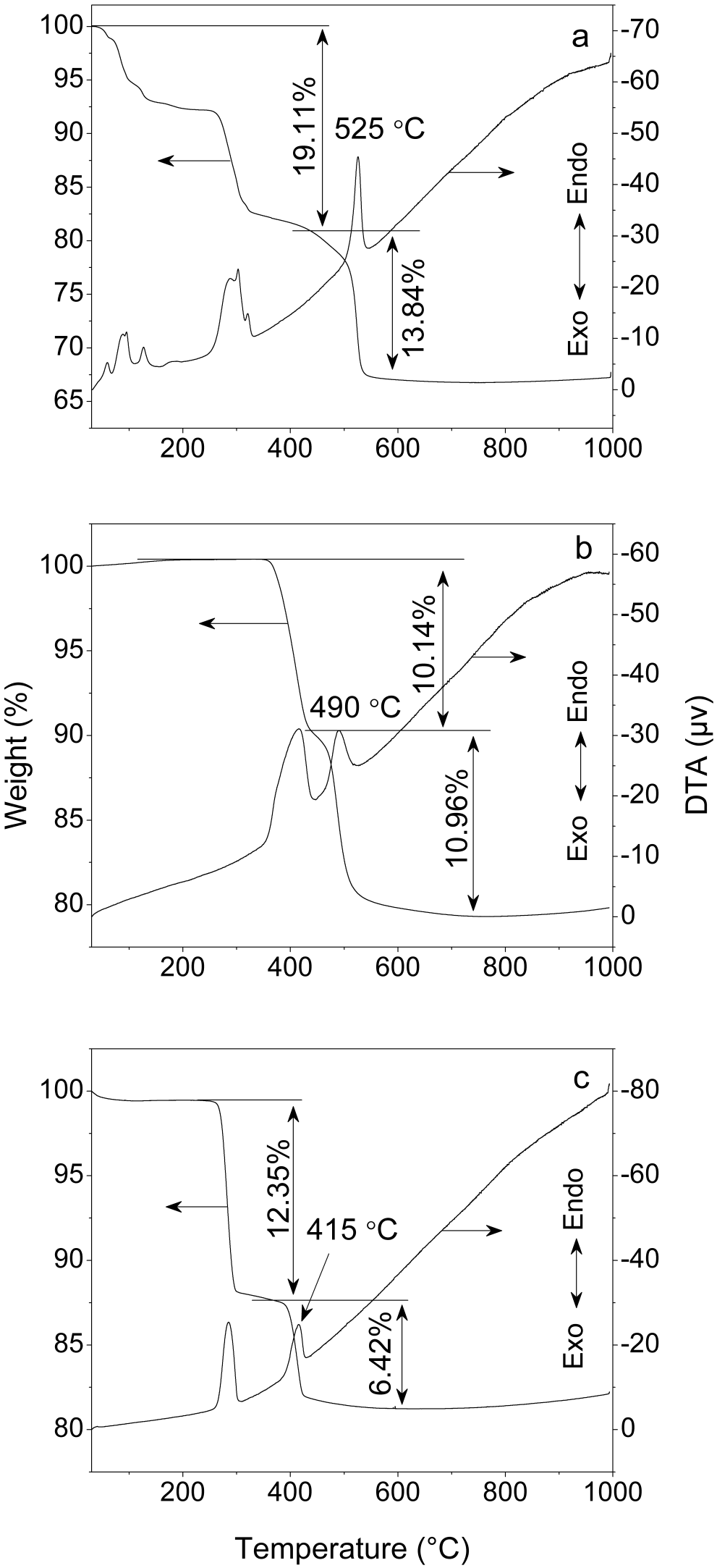
a
19.11%
525 °C
13.84%
Endo
Exo
b
10.14%
490 °C
10.96%
Endo
Exo
c
12.35%
415 °C
6.42%
Endo
Exo
Weight (%)
DTA (μv)
Temperature (°C)

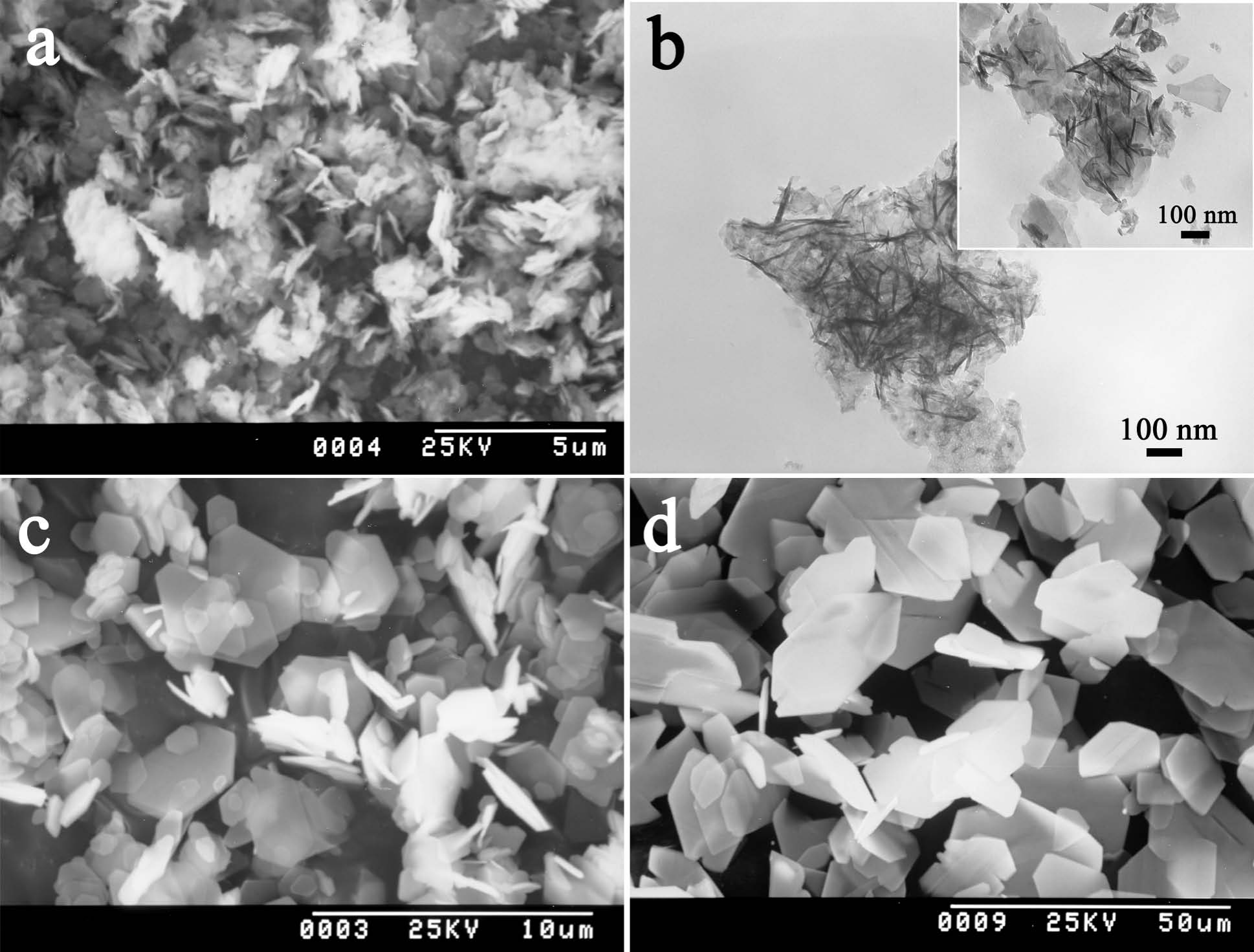
a
0004 25KV 5um
b
100 nm
100 nm
c
0003 25KV 10um
d
0009 25KV 50um

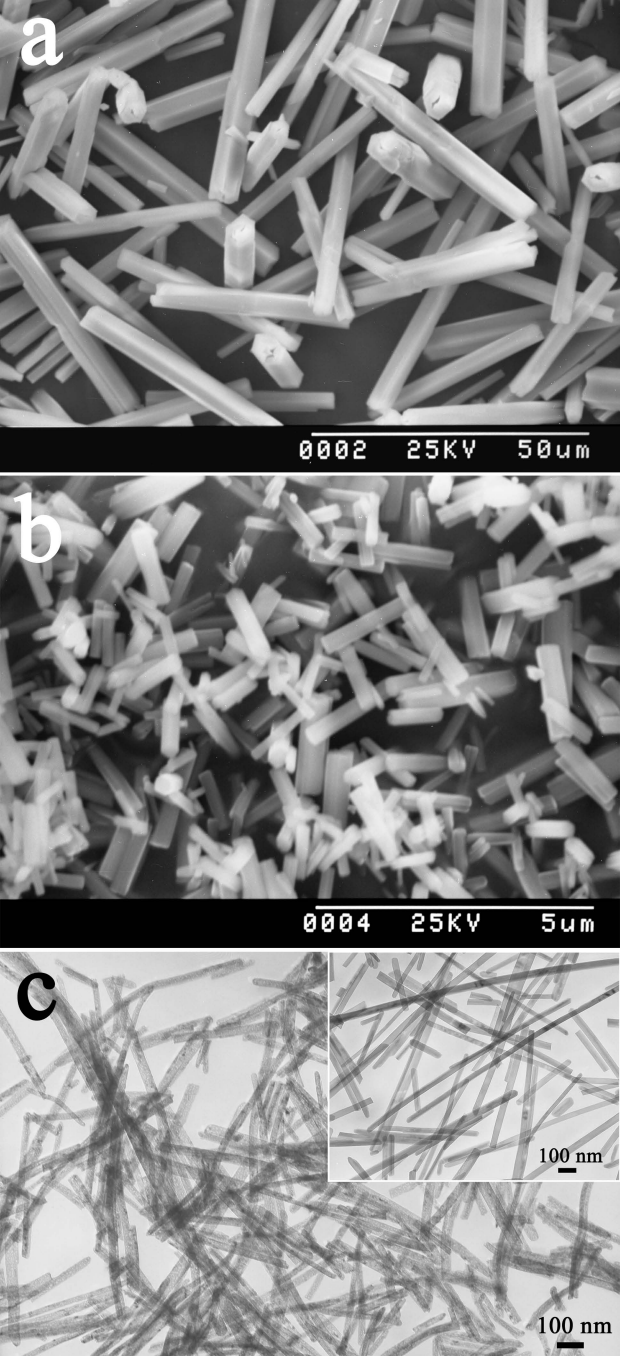
a
0002 25KV 50um
b
0004 25KV 5um
c
100 nm
100 nm

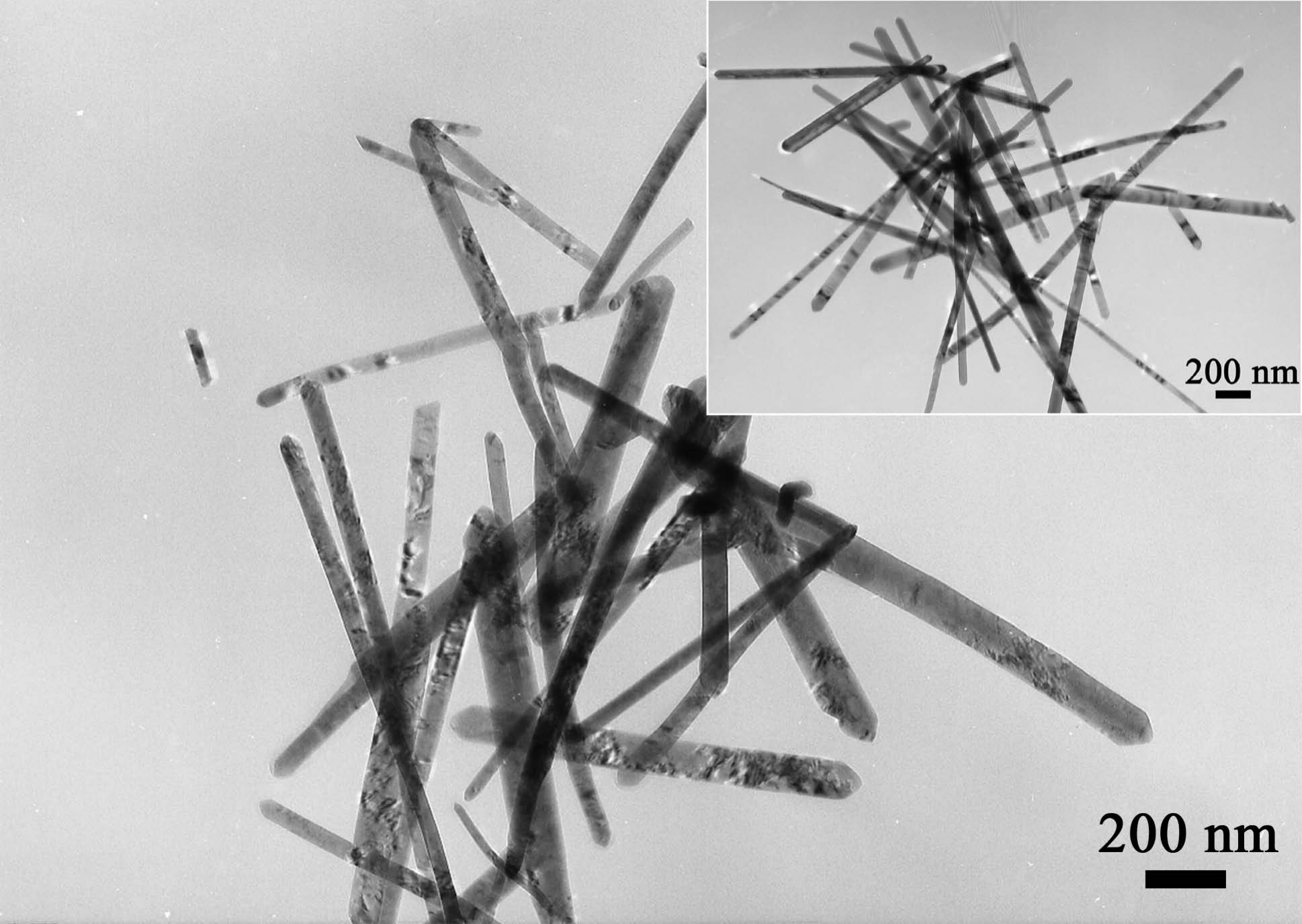
200 nm
200 nm

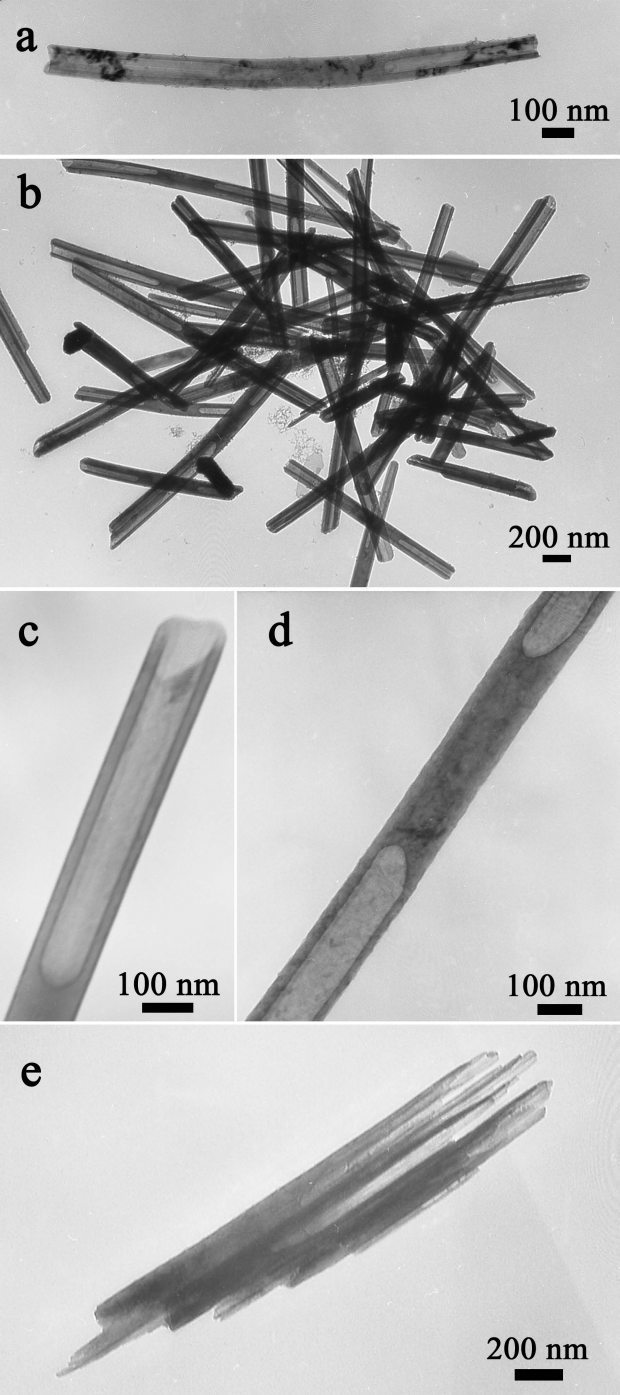
a
100 nm
b
200 nm
c
100 nm
d
100 nm
e
200 nm